

# Cycloidal Trajectory Realization on Staircase with Optimal Trajectory Tracking Control based on Neural Network Temporal Quantized Lagrange Dynamics (NNTQLD)

Gaurav Bhardwaj<sup>1,†,\*</sup>, Utkarsh A. Mishra<sup>2,†</sup>, N. Sukavanam<sup>3</sup> and R. Balasubramanian<sup>1</sup>

**Abstract**—In this paper, a novel optimal technique for joint angles trajectory tracking control of a biped robot with toe foot is proposed. For the task of climbing stairs by a 9 link biped model, a cycloid trajectory for swing phase is proposed in such a way that the cycloid variables depend on the staircase dimensions. Zero Moment Point(ZMP) criteria is taken for satisfying stability constraint. This paper mainly can be divided into 4 steps: 1) Planning stable cycloid trajectory for initial step and subsequent step for climbing upstairs. 2) Inverse Kinematics using unsupervised artificial neural network with knot shifting procedure for jerk minimization. 3) Modeling Dynamics for Toe foot biped model using Lagrange Dynamics along with contact modeling using spring damper system, and finally 4) Real time joint angle trajectory tracking optimization using Temporal Quantized Lagrange Dynamics which takes inverse kinematics output from neural network as its inputs. Generated patterns have been simulated in MATLAB ®.

## I. INTRODUCTION

The functional planning of legged robots is often derived by animals evolved to excel at the required tasks. However, while imitating such naturally occurring features seen in nature can be very powerful, robots may need to perform several complicated motor tasks that their living counterparts do not. In this context, the most advanced robots which aim towards achieving human-like motion are bipedal robots and humanoids. Different motion patterns of humanoid and biped robots have recently been an active field of research. Walking, running, jogging, ascending and descending stairs and slopes are among the most important ones and can consequentially demonstrate the adaptability of such robots to the surrounding environment. Also, despite wheeled robots, biped robots have a better ability to move on uneven grounds or other complex environments. However, there are some challenges with such systems along with the advantages accompanying it. The dynamics of these robots are complex and inherently unstable. Furthermore, numerous gait patterns have been considered for such types of robots, however, due to the high number of Degrees of Freedom (DOF) of such robots, these methods are not generalizable and each one focuses on realizing a specific gait.

<sup>1</sup>Gaurav Bhardwaj and R.Balasubramanian are with the Computer Science and Engineering Department, IIT Roorkee [gbhardwaj@cs.iitr.ac.in](mailto:gbhardwaj@cs.iitr.ac.in), [balarfcs@iitr.ac.in](mailto:balarfcs@iitr.ac.in)

<sup>2</sup>Utkarsh A. Mishra is with the Mechanical and Industrial Engineering Department, IIT Roorkee [umishra@me.iitr.ac.in](mailto:umishra@me.iitr.ac.in)

<sup>3</sup>N. Sukavanam is with the Mathematics Department, IIT Roorkee [nsukvfma@iitr.ac.in](mailto:nsukvfma@iitr.ac.in)

<sup>†</sup> These authors have contributed equally.

\* Corresponding Author

## II. RELATED WORK

Many researchers proposed the trajectory generation and control algorithm for the biped robots on flat surfaces [1], [2], [3]. Moreover, studies about the ascending or descending stairs by these robots have been a subject of active research [4], [5], [6]. Kajita et al. [2] suggested preview control of Zero Moment Point with a spiral staircase. Park et al. have presented a trajectory generation method and control approach for a biped robot to climb stairs [5]. They developed an off-line path planning method using the Virtual Height Inverted Pendulum Model (VHIPM) method. Shih and Chio [7] studied stairs walking for biped robot taking static models. Jeon et al. [8] proposed a genetic algorithm-based optimal trajectory generation method to walk upstairs. Morisawa et al. [9] pattern generation technique for biped walking constraint on a parametric surface. Sato et al. [10] proposed a virtual slope method for biped robot climbing on stairs. Gutmann [11] proposed a stereo vision technique for a humanoid robot to climb stairs. Significant methods presented in the literature are designed based on a predefined path tracking. However, when the environment changes, it is necessary to redesign the trajectory. Nevertheless, humans do not walk based on a predefined trajectory. Humans predict their next steps based on several environmental and geometric constraints.

In order to achieve effective knowledge and formulate proper tracking measures, robot dynamics and kinematics play a crucial role. For specifically, in such tracking problems, Inverse Kinematics has been an active field of concern. Artificial neural networks(ANN) played a significant role in robots and manipulators in the past decades. When talking about inverse kinematics, artificial neural networks give more satisfying results compared to geometric, iterative, or analytic methods, the reason being the existence of multiple solutions in case of inverse kinematics. [12], [13], [14], [15], [16], [17] used a supervised neural network for inverse kinematics solution obtaining training data from the relationship between joint coordinates and end effector Cartesian coordinates. Panwar [18] applied the ANN method for bipedal stable walking without obtaining training data in an unsupervised manner. For biped robot dynamics, either we can approximate our model by taking simplified cases like Inverted Pendulum Model [19], [20], [21], [22] for the purpose of trajectory generation. On the other hand, we can take distributed mass to develop dynamic equations as well.

Also, because of the unilateral contact between a humanoid robot foot and the terrain surface, the walking patterns should fulfill certain feasibility constraints as well. These are funda-

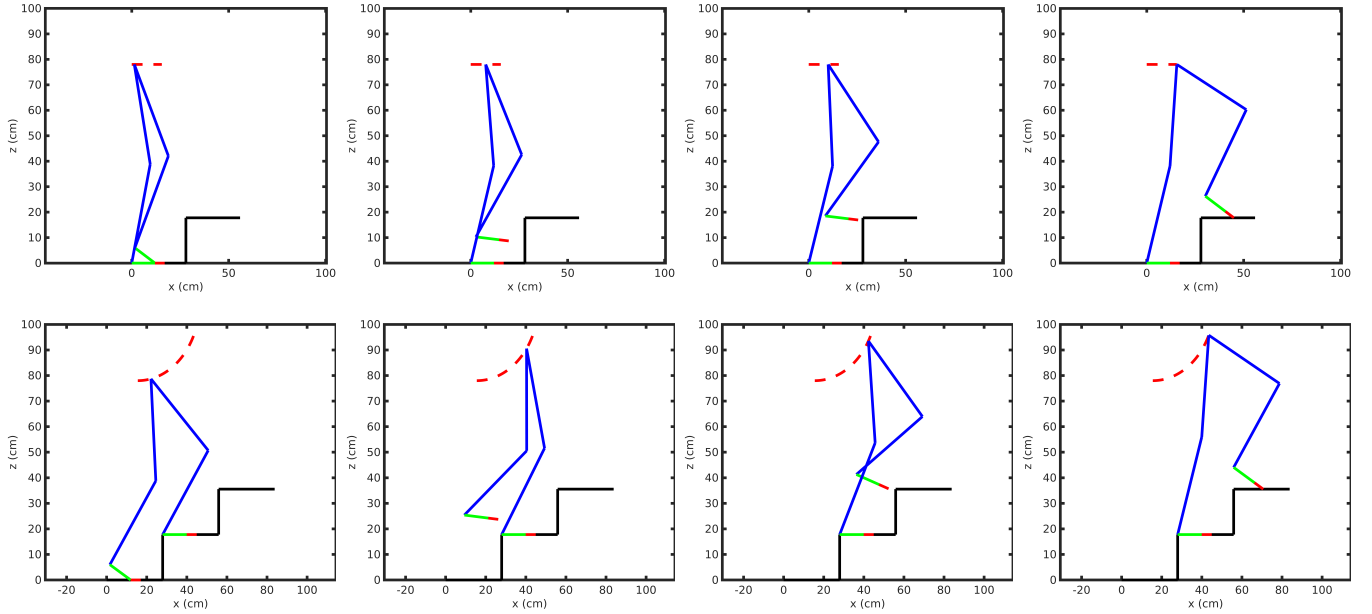


Fig. 1. Motion Instants for Proposed Upstairs Climbing Strategy

mental constraints that ensure stability and hence make them walk on flat or rough terrains without falling down. Vukobratovic [23] in 1972 proposed a measuring index for stability called Zero Moment Point. Foot Rotation Indicator (FRI) [24] is another technique that determines the tendency of feet to rotate. Hirukawa [25] proposed the Contact Wrench sum and Contact Wrench Cone approached to work as an indicator of stability in biped robots. ZMP is one of the simplest and most used techniques.

### III. CONTRIBUTION OF PRESENTED WORK

In this paper, a novel cycloidal realization is performed to accomplish stair climbing by a toe-foot biped robot model. Furthermore, to complete the trajectory tracking objectives, ANN-based kinematics and dynamics algorithm was formulated to structure the torque profiles and hence providing evidence to shed some light on the energy consumption and power requirements as well. The paper incorporates the following contributions:

The cycloidal trajectory proposed in the work is dynamic in nature and hence can easily adapt to the changing stair geometry and for various robot dimensions. In the case of staircases, the optimal rise/run ratio is about  $11/7 = 1.57$  [26], which is one of the reasons for taking cycloid as reference trajectory for the swing phase because for half of cycloid, horizontal to vertical distance ratio is  $\pi/2 = 1.57$  which is an unnoticed fact. This is in complete congruence with the fact dynamic planning strategy humans adapt. The desired trajectory is composed of multiple segments such that the robot plans, catches, and tracks a cycloidal trajectory. Parameters of the cycloid are based on the configuration of the staircase and the algorithm for calculation of ankle trajectory is developed which is applicable for varying staircase dimensions which

make it computationally faster compared to polynomial based techniques. A circular arc trajectory is considered for the hip.

A novel online trajectory tracking procedure is developed where an ANN-based real-time unsupervised inverse kinematics is performed and the processed output is served as the desired joint space variables for a trajectory tracking algorithm. The tracking algorithm is based on a novel temporally quantized classical Euler-Lagrangian dynamics with a distributed mass model approach which enables the trajectory tracker to choose the desired torques in order to satisfy extra constraints while following the desired trajectory to the maximum extent. The approach starts with quantizing time by taking a suitable time step throughout the pre-calculated ankle trajectory for climbing staircase step, then for every two consecutive ankle position  $i$  and  $(i+1)$ , where  $i: 0, 1, \dots, n$ :  $n$  denotes total number of time instants, UIKNN provides joint angle variables which are then fed into trajectory tracker to get torque values for  $i^{th}$  instant and the same procedure is repeated throughout the trajectory to get real-time torque values. The complete methodology takes place in real-time where the inverse kinematics jointly enables the robot to follow the desired trajectory as well as maintain stability. Thus, the overall methodology can be termed as a Neural Network Temporal Quantized Lagrangian Dynamics (NNTQLD) approach.

This paper is organized as follows: Section II describes the considered toe foot, robot model. Section III is dedicated to staircase trajectory planning for robot followed by ANN-based inverse kinematics solution in section IV. Section V elaborated our contact model and then Dynamic Modeling for the robot in Section VI which elaborated both Lagrange Dynamics and TQLD approach. Section VII describes the ZMP stability criteria. Section VIII is dedicated to trajectory tracking optimization. Finally, in section IX, the obtained results are analyzed and the paper concludes the whole procedure in

section X.

#### IV. ROBOT MODEL DESCRIPTION

The model considered for the work is a planar biped with a toe-foot joint. The motion is completely constrained to the sagittal plane. Each leg consists of 4 links and 4 joints, all of which are revolute in nature as shown in Fig. 2. These joints are referred as the Hip(H), Knee(K), Ankle(A), Sole(S) along with the Toe tip(T). The attributes of the model can be visualized from Fig. 2 and is shown in Table I.

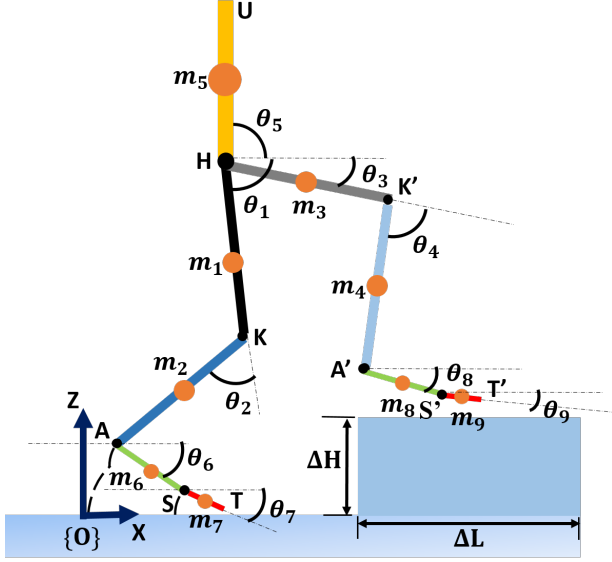


Fig. 2. Toe-Foot Robot Model Description and Notations

TABLE I  
JOINT POSITIONS AND ATTRIBUTES OF EACH LINK

Joint Name	Positions				
Hip(H)	H (both Swing & Stance Leg)				
Knee(K)	K (Swing Leg), K' (Stance Leg)				
Ankle(A)	A (Swing Leg), A' (Stance Leg)				
Sole(S)	S (Swing Leg), S' (Stance Leg)				
Toe(T)	T (Swing Leg), T' (Stance Leg)				
Link No.	Link	Length	Value(cm)	Mass	Value(Kg)
1	HK	$l_1$	40	$m_1$	6
2	KA	$l_2$	40	$m_2$	4
3	HK'	$l_3$	40	$m_3$	6
4	K'A'	$l_4$	40	$m_4$	4
5	UH	$l_5$	30	$m_5$	30
6	AS	$l_6$	12	$m_6$	0.70
7	ST	$l_7$	5	$m_7$	0.15
8	A'S'	$l_8$	12	$m_8$	0.70
9	S'T'	$l_9$	5	$m_9$	0.15

Thus, the total length of the leg is  $(l_1 + l_2)$  and that of foot is  $(l_5 + l_6)$ . For a gait, the model hip is treated as the base and the ankle of the active leg is considered as the end-effector and this corresponds to a 2-link manipulator. The movement is divided into 2 phases, namely the Double Support Phase (DSP) and the Single Support Phase (SSP). The former one corresponds to the initial condition when both the feet are making contact

with the ground whereas the latter represents the swing of the active leg with passive leg's foot remaining in contact with the ground.

The presented work explores the possibilities of stable stair climbing for the model shown with known variable step length and height. The complete task objective is as follows:

1. Consider a standing position, the model starts to climb the first step of the staircase, attains a velocity.
2. Second task objective is to enable the model to climb alternate steps in such a way to minimize the actuator effort.

#### V. TRAJECTORY PLANNING

##### A. For Swing Leg

The biped is considered to be planar as visualized from the sagittal plane only. The torso movement is not considered. A complete motion is achieved during the time interval  $(t_0 = 0, t_f)$ , which is divided into majorly four phases.

- $t = 0$  to  $t_2$ : Double Support Phase
- Single Support Phase - Pick the Cycloid
- $t = t_2$  to  $t_{bc}$ : Single Support Phase - Catch the Cycloid
- $t = t_{bc}$  to  $t_f$ : Single Support Phase - Track the Cycloid

Each phase is described as follows:

1) *Double Support Phase*: The feet of the swing leg denoted by points A, S and T are on the ground with coordinates  $(0, 0)$ ,  $(l_6, 0)$  and  $(l_6 + l_7, 0)$  respectively. The feet is considered to move as a two-link manipulator with AS and ST as the two arms about the fixed toe, T.

Thus, during this phase, the ankle coordinates are given by the following equations.

$$x_A(t) = l_6(1 - \cos\theta_6) + l_7(1 - \cos\theta_7) \quad (1)$$

$$z_A(t) = l_6 \sin\theta_6 + l_7 \sin\theta_7 \quad (2)$$

For the duration, the sole AS rotates about S, from angle 0 at  $t = 0$  to angle  $\theta_a$  at time  $t = t_1$  with toe being stable on ground. For the time duration,  $(t_1, t_2)$  the AS-ST links behave as 2 link manipulator about T where AS reverses its motion and ST rotates from angle 0 at  $t = t_1$  to angle  $\theta_b$  at time  $t = t_2$ . The parameters  $\theta_a$  and  $\theta_b$  are modeling parameters for stable gait generation. Thus, for polynomial parametrization of the motion,

$$\theta_6(t) = \begin{cases} \theta_a(3\frac{t^2}{t_1^2} - 2\frac{t^3}{t_1^3}), & \text{if } 0 \leq t \leq t_1 \\ \theta_a(-4 + 12\frac{t}{\Delta t_{DSP}} - 9\frac{t^2}{\Delta t_{DSP}^2} + 2\frac{t^3}{\Delta t_{DSP}^3}), & \text{if } t_1 \leq t \leq t_2 \end{cases} \quad (3)$$

$$\theta_7(t) = \begin{cases} 0, & \text{if } 0 \leq t \leq t_1 \\ \theta_b(-5 + 12\frac{t}{\Delta t_{DSP}} - 9\frac{t^2}{\Delta t_{DSP}^2} + 2\frac{t^3}{\Delta t_{DSP}^3}), & \text{if } t_1 \leq t \leq t_2 \end{cases} \quad (4)$$

where,  $\Delta t_{DSP} = t_2 - t_1$ .

2) *Single Support Phase - Pick the Cycloid*: Cycloidal trajectory planning enables null accelerations at the beginning and the end of the gait and hence, the dynamic forces on the links are not significant for those instants. Furthermore, the smooth change in accelerations results to suitable behavior of the dynamic forces contributing to stable gaits. The trajectory

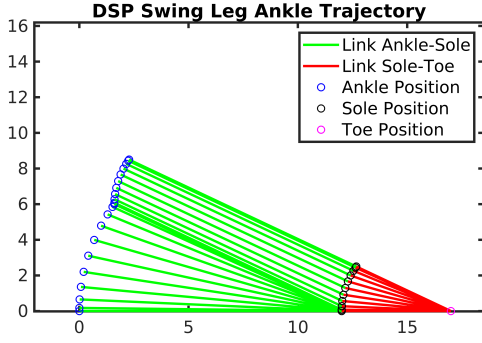


Fig. 3. Swing leg's Foot Trajectory during DSP

parameters used for the study is based on the robot's geometrical as well as the task objective discussed in the model description section.

Let us consider a cycloid of constant radius  $r$  and a time parametrized  $\theta(t)$ , on which the Cartesian coordinates of a point is given by,

$$x_{cycloid}(t) = r(\theta_c(t) - \sin \theta_c(t)) \quad (5)$$

$$z_{cycloid}(t) = r(1 - \cos \theta_c(t)) \quad (6)$$

The maximum height that can be achieved in such a motion is at  $\theta = \pi$  which is at a horizontal distance of  $\pi r$ . Now, to climb any step of height ( $\Delta z$ ) and at certain distance ( $\Delta x$ ),  $r$  is considered to be equal to  $\Delta z/2$  and cycloid is formed with the height of the ankle  $z_A(t_2)$ , at the end of DSP, as its origin height and a variable  $x_{c0}$  coordinate depending upon the step parameters. The starting of the cycloid is governed by the value of  $\theta_c$  at the beginning. After the DSP ends, the remaining distance to be covered by the trajectory happens to be  $\Delta x_c = (\Delta x - x_A(t_2))$ . The value of  $\theta_c$  in the beginning,  $\theta_{c0}$ , is chosen such that it satisfies,

$$r(\theta_{c0} - \sin \theta_{c0}) = \pi r - \Delta x_c, \quad (7)$$

if  $\pi r \geq \Delta x_c$  and 0 otherwise. (7) shows the dependence of the value of  $x_{c0}$  on  $r$  and  $\Delta x_c$ . As the DSP is bounded by the workspace and feasibility constraints of a 2-link mechanism, it becomes difficult for it to follow the above described cycloidal trajectory just after it ends and hence, there should be a bridge to catch the cycloid after the DSP ends.

3) *Single Support Phase - Catch the Cycloid:* This bridge is modeled as a bezier curve. The trajectory was formulated based on 4 control points, namely  $(x_{c_i}^b, z_{c_i}^b)$  for  $i = 1$  to 4, which starts from the end of DSP i.e.  $(x_{c1}^b, z_{c1}^b) = (x_A(t_2), z_A(t_2))$  being the first control point. The second control point was chosen based on the cycloid formulation, with the value of  $\theta_{c0}$ .

$$x_{c2}^b = \begin{cases} x_A(t_2), & \text{if } \pi r \geq \Delta x_c \\ (\Delta x - \pi r), & \text{otherwise} \end{cases} \quad (8)$$

$$z_{c2}^b = \begin{cases} z_A(t_2) + r(1 - \cos \theta_{c0}), & \text{if } \pi r \geq \Delta x_c \\ z_A(t_2), & \text{otherwise} \end{cases} \quad (9)$$

The remaining control points were selected from within the cycloid such that the bezier curve blends completely with the

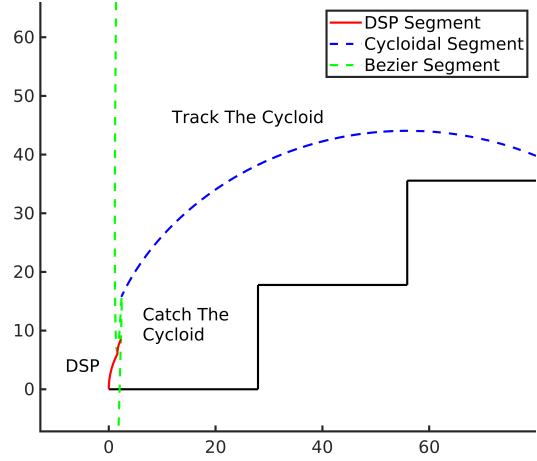


Fig. 4. Various Segments of Swing Leg's Ankle Trajectory Planning for Subsequent Upstairs Climbing

cycloidal trajectory. Considering that the bezier curve catches the cycloid in time  $t_{bc}$ , the other two control points were chosen to be at an angular displacement of  $\theta_{c3}^b = \theta_{c0} + \Delta\theta_{c0}$  and  $\theta_{c4}^b = \theta_{c0} + 2\Delta\theta_{c0}$  respectively, such that the coordinates  $(x_{c3}^b, z_{c3}^b)$  and  $(x_{c4}^b, z_{c4}^b)$  are obtained from the cycloid equation given in (5) and (6). Finally, the bezier curve is determined to be,

$$x^b(t) = (1-s)^3 x_{c1}^b + (1-s)^2 s x_{c2}^b + (1-s)s^2 x_{c3}^b + s^3 x_{c4}^b \quad (10)$$

$$z^b(t) = (1-s)^3 z_{c1}^b + (1-s)^2 s z_{c2}^b + (1-s)s^2 z_{c3}^b + s^3 z_{c4}^b \quad (11)$$

where  $s = \frac{t-t_2}{t_{bc}-t_2}$  is the normalized time in the duration for which the ankle traverses the bezier curve trajectory. Furthermore, to maintain the continuity the velocity at the blend of the bezier and cycloid curves should be same, hence

$$\dot{\theta}_c(t = t_{bc}) = \frac{\dot{z}^b(t = t_{bc})}{r \sin \theta_{c4}^b} \quad (12)$$

Also, to make the complete utilization of cycloidal trajectory,  $\ddot{z}_c(\theta_c = \pi) = g$ , where  $g$  is the acceleration due to gravity. This deduces to  $\theta_c(t = t_3) = \sqrt{g/r}$ . Finally, the complete cycloid definition can be completed by defining  $\theta_c(t)$  as,

$$\theta_c(t) = a_{c0} + a_{c1}t + a_{c2}t^2 + a_{c3}t^3, \quad (13)$$

where the coefficients  $a_{c_i}$ 's are given by,

$$\begin{bmatrix} \theta_{c4}^b \\ \dot{\theta}_c(t = t_{bc}) \\ \pi \\ \dot{\theta}_c(t = t_3) \end{bmatrix} = \begin{bmatrix} 1 & t_{bc} & t_{bc}^2 & t_{bc}^3 \\ 0 & 1 & 2t_{bc} & 3t_{bc}^2 \\ 1 & t_3 & t_3^2 & t_3^3 \\ 0 & 1 & 2t_3 & 3t_3^2 \end{bmatrix} \begin{bmatrix} a_{c0} \\ a_{c1} \\ a_{c2} \\ a_{c3} \end{bmatrix} \quad (14)$$

4) *Movement of Sole and Toe:* The trajectory of the sole (S) and toe (T) during the complete motion ( $0 \leq t \leq t_3$ ) were chosen based on the geometry of the robot and the stair-step with which it is interacting. It was assured that no collision with the surface occurs at any point. The  $x$  and  $z$  coordinates of S and T are given by the following equations.

$$x_T(t) = \begin{cases} l_6 + l_7, & \text{if } 0 \leq t \leq t_2 \\ x_A(t) + (l_6 + l_7) \cos \theta_6(t), & \text{if } t_2 \leq t \leq t_3 \end{cases} \quad (15)$$

---

**Algorithm 1: Swing Leg Trajectory Planning**


---

**Result:** Pick and Catch the Cycloid  
 Given  $\Delta x, \Delta z, x_A(0), z_A(0), x_A(t_f), z_A(t_f)$ ;  
 Initialize  $r = \Delta z/2, \theta_c(t_f) = \pi, \Delta\theta_{c0} = 0.01rad$ ;  
**while**  $t \leq t_2$  **do**  
 | Perform DSP from Ankle from  $(x_A(0), z_A(0))$  to  
 |  $(x_A(t_2), z_A(t_2))$ ;  
**end**  
 Fix Cycloid with  $r, \theta_c(t_f)$ ;  
 Cycloid Ankle Position  $(\theta_c = \theta_{c0}) = (x_A(t_f), z_A(t_f))$ ;  
**if**  $\pi r \geq \Delta x_c$  **then**  
 | Solve  $r(\theta_{c0} - \sin \theta_{c0}) = \pi r - \Delta x_c$  to get  $\theta_{c0}$   
**else**  
 |  $\theta_{c0} = 0$   
**end**  
**while**  $t_2 < t \leq t_{bc}$  **do**  
 | Perform Bezier Curve with 4 control points  
 |  $(x_{c1}^b, z_{c1}^b)$  at DSP  
 |  $(x_{c2}^b, z_{c2}^b)$  at  $\theta_c = \theta_{c0}$   
 |  $(x_{c3}^b, z_{c3}^b)$  at  $\theta_c = \theta_{c0} + \Delta\theta_{c0}$   
 |  $(x_{c4}^b, z_{c4}^b)$  at  $\theta_c = \theta_{c0} + 2\Delta\theta_{c0}$ ;  
**end**  
**while**  $t_{bc} < t \leq t_f$  **do**  
 | Perform Cycloid for Ankle from  
 |  $\theta_c = \theta_{c0} + 2\Delta\theta_{c0}$  to  
 |  $\theta_c = \theta_c(t_f) = \pi$ ;  
**end**

---

$$z_T(t) = \begin{cases} 0, & \text{if } 0 \leq t \leq t_2 \\ z_A(t) + (l_6 + l_7) \sin \theta_6(t), & \text{if } t_2 \leq t \leq t_3 \end{cases} \quad (16)$$

$$x_S(t) = \begin{cases} l_6, & \text{if } 0 \leq t \leq t_1 \\ l_6 + l_7 - l_7 \cos \theta_7(t), & \text{if } t_1 \leq t \leq t_2 \\ x_A(t) + l_3 \cos \theta_6(t), & \text{if } t_2 \leq t \leq t_3 \end{cases} \quad (17)$$

$$z_S(t) = \begin{cases} 0, & \text{if } 0 \leq t \leq t_1 \\ l_7 \sin \theta_7(t), & \text{if } t_1 \leq t \leq t_2 \\ z_A(t) + l_6 \sin \theta_6(t), & \text{if } t_2 \leq t \leq t_3 \end{cases} \quad (18)$$

Here,

$$\theta_3(t) = a_{t30} + a_{t31}t + a_{t32}t^2 + a_{t33}t^3, \quad (19)$$

for  $t = (t_2, t_3)$ , where the coefficients  $a'_{t3i}$ s are given by,

$$\begin{bmatrix} \theta_b \\ 0 \\ \theta_b \\ 0 \end{bmatrix} = \begin{bmatrix} 1 & t_2 & t_2^2 & t_2^3 \\ 0 & 1 & 2t_2 & 3t_2^2 \\ 1 & t_3 & t_3^2 & t_3^3 \\ 0 & 1 & 2t_3 & 3t_3^2 \end{bmatrix} \begin{bmatrix} a_{t30} \\ a_{t31} \\ a_{t32} \\ a_{t33} \end{bmatrix} \quad (20)$$

Once, the swing leg lands with its toe (T) touching the ground, the next DSP phase starts and the ankle follows the exact reverse trajectory of that discussed in the first part of this segment i.e. first as a 2-link manipulator with fixed axis at T and then a single link manipulator with fixed axis at sole (S).

### B. For Hip Motion

The motion of the hip was formulated as a COG trajectory with the ZMP equation of a one-mass COG model in sagittal plane. During the single support phase, the analytical solution of ZMP trajectory is considered as the COG trajectory. Additionally, the ZMP motion is planned as a 3-degree polynomial parametrization with C-2 continuity. For such a formulation, the ZMP trajectory in sagittal plane is as follows.

$$p_x(t) = x_C(t) - \frac{z_C}{g} \ddot{x}_C(t) \quad (21)$$

$$p_x(t) = a_{z0} + a_{z1}t + a_{z2}t^2 + a_{z3}t^3 \quad (22)$$

where  $(p_x(t), 0)$  and  $(x_C, z_C)$  represent the ZMP and COG position respectively. The analytical solution for the ZMP equations (21) and (22), and the COG trajectories is obtained as follows,

$$x_C(t) = C_1 e^{\omega t} + C_2 e^{-\omega t} + a_{z0} + a_{z1}t + a_{z2}t^2 + a_{z3}t^3 + \frac{z_C}{g} (6a_{z3}t + 2a_{z2}) \quad (23)$$

$$\omega = \sqrt{\frac{g}{z_{Ci}}} \quad (24)$$

where,  $z_{Ci}$  is the initial centroidal height. Various researches have used COG trajectory for the z-direction in the form of a virtual slope given by  $z_C(t) = kx_C(t) + z_{Ci}$  where the value of  $k$  is determined based on the slope of the stairs step need to be climbed [26]. But, such an approximation is not practical for determining the hip motion. Hence, the hip motion is modeled as a circular arc with the virtual slope trajectory as its chord length. This inverted circular arc traverses between the initial hip position  $(x_H^{initial}, z_H^{initial})$  to the final hip position  $(x_H^{final}, z_H^{final})$  in a more practical manner. Let  $R_H$  and  $\theta_H$  denote the segment corresponding to the desired arc.

$$\begin{aligned} R_H \sin(\theta_H) &= x_H^{final} - x_H^{initial} \\ R_H (1 - \cos(\theta_H)) &= z_H^{final} - z_H^{initial} \end{aligned} \quad (25)$$

$$z_C(t) = z_{Ci} + \sqrt{R_H^2 - (x_C(t) - x_H^{initial})^2}$$

Furthermore, the value of coefficients  $a'_{zi}$ s,  $C_1$  and  $C_2$  in equation (23) is determined using the boundary conditions of ZMP and COG respectively for the time-interval  $(0, t_3)$ . These boundary conditions are given in the following equations.

$$\begin{bmatrix} x_{ZMP}^{initial} \\ 0 \\ x_{ZMP}^{final} \\ 0 \end{bmatrix} = \begin{bmatrix} 1 & 0 & 0 & 0 \\ 0 & 1 & 0 & 0 \\ 1 & t_3 & t_3^2 & t_3^3 \\ 0 & 1 & 2t_3 & 3t_3^2 \end{bmatrix} \begin{bmatrix} a_{z0} \\ a_{z1} \\ a_{z2} \\ a_{z3} \end{bmatrix} \quad (26)$$

$$x_C(t=0) = x_{COG}^{initial}, x_C(t=t_3) = x_{COG}^{final}$$

### C. For Stance leg

The stance leg follows the hip trajectory while keeping the ankle fixed. Furthermore, the sole (S') and toe (T') of stance leg remain at the same point. As the swing leg starts DSP for the next phase, the DSP for stance leg commences. The planning for this motion is similar, although, the planning next place for the next intermediate step.

## VI. INVERSE KINEMATICS

### A. Inverse Kinematics formulation

For forward kinematics we have used equation from [13] based on D-H Procedure. The previous trajectory planning segment clearly defines the trajectory of the hip (H), ankle (A), sole (S) and toe (T). Considering hip (H) as the base and ankle (A) as the end-effector, the forward kinematics equation is obtained as a function of the joint angles  $\theta_1(t)$  and  $\theta_2(t)$ .

$$x_A(t) = x_H(t) + (l_1 \cos \theta_1(t) + l_2 \cos(\theta_1(t) + \theta_2(t))) \quad (27)$$

$$z_A(t) = z_H(t) - (l_1 \sin \theta_1(t) + l_2 \sin(\theta_1(t) + \theta_2(t))) \quad (28)$$

The equations (26) and (27) apply for both the swing leg and the stance leg with joint angles  $\theta_1(t), \theta_2(t)$  and  $\theta_5(t), \theta_6(t)$  respectively.

### B. Knot shifting procedure based Unsupervised Inverse Kinematics Neural Network (UIKNN) approach

1) *UIKNN*: An ANN based approach was used to solve the inverse kinematics problem from the forward kinematic equations (27) and (28). A feed forward network was modeled and trained in real time for every time instant. The hyperparameters of the network are given in Table II. For a desired

TABLE II  
HYPERPARAMETERS FOR FEED FORWARD NETWORK

Parameter	Value
Input Neurons	2
Output Neurons	2
Hidden layer	1
Hidden layer nodes	10
Activation function	Sigmoid $1/(1+e^{-x})$
Learning Rate	$10^{-4}$
Maximum Iterations	5000

ankle position  $(x_A^{input}, z_A^{input})$ , the joint angles  $\theta_1^{network}$  and  $\theta_2^{network}$  were approximated. These approximated joint angles were substituted in the (27) and (28) to obtain the network estimated ankle position  $(x_A^{network}, z_A^{network})$ . Finally, the loss (error) function,  $E_{network}$ , was calculated as the squared error between the desired and approximated ankle positions.

$$E_{network} = (x_A^{input} - x_A^{network})^2 + (z_A^{input} - z_A^{network})^2 \quad (29)$$

The loss function was optimized using a gradient descent based on the partial differentiation of the error with respect to the layer weights. Finally, the weights ( $W$ ) were updated according to the calculated gradients ( $\delta$ ), for each time step i.e.

$$W_{n+1}(t) = W_n(t) - \alpha \delta, \quad (30)$$

where  $n$  represents the iteration (epoch) number. The weight updates were stop once the error goes down below the threshold equal to  $10^{-6}$ .

---

### Algorithm 2: UIKNN Algorithm

---

**Result:** Unsupervised Inverse Kinematics Neural Network

*Determine* coordinates of Hip(H), Ankle(A);

$W_{ij} \leftarrow$  Hidden Layer Weights;

$W_{jk} \leftarrow$  Output Layer Weights;

$W_{ij}, W_{jk} \leftarrow$  Random Initializing;

$Act() \leftarrow$  Sigmoid Activation function;

$\alpha \leftarrow$  learning rate;

**while**  $t \leq t_{final}$  **do**

\leftarrow (A)[x, y] ;

    output  $[\theta_1, \theta_2] \leftarrow W_{jk}(Act(W_{ij} * input))$ ;

$(A)_{modified} \leftarrow function((H), \theta_1, \theta_2)$  **from** (27) (28);

    Error( $E$ )  $\leftarrow (A)_{modified} - (A)$  **from** (29);

**if**  $(E) \leq 10^{-6}$  **then**

        | Stop;

**else**

$\delta_{ij}, \delta_{jk} \leftarrow \partial E / W_{ij}, \partial E / W_{jk}$ ;

$W_{ij} \leftarrow W_{ij} - \alpha \delta_{ij}$ ;

$W_{jk} \leftarrow W_{jk} - \alpha \delta_{jk}$ ;

**end**

**end**

---

2) *Knot Shifting Procedure*: In case of bipedal robot or for a general manipulator also, joint space trajectory demands for jerk free trajectory so that basic equations of motion are valid which are applicable in case of uniform acceleration. First two equations of motion with non zero jerk are given by:

$$v = u + at + 1/2jt^2 \quad (31)$$

and

$$s = ut + 1/2at^2 + 1/6jt^3 \quad (32)$$

where  $s, v, u, a, j, t$  denotes displacement, final velocity, initial velocity, acceleration, jerk and time respectively. To neglect the jerk term we can minimize the  $t$  which we are doing by temporal quantization with  $\Delta t = 0.01$  and we must also keep value of  $j$  as minimum as possible for which we are applying knot shifting procedure.

The trajectory planning section is governed by various parameters which can be changed in order to achieve optimal solution based on a suitable objective function. Furthermore, analysis over a complete trajectory seems futile and optimization at knot-points are enough to achieve the desired optimal solution. With these considerations and an objective function based on minimization of the absolute jerk faced in joint space, knot shifting procedure was implemented, as in Fig. 5, such that a trajectory with relatively minimum jerk can be obtained. The aim of such an approach is to choose the governing parameters based on some real life applicable objectives and serves as an add-on to the trajectory planning methodology proposed in the study. Thus, suitable values of the parameters after implementing knot shifting are given in Section IX in Table III.

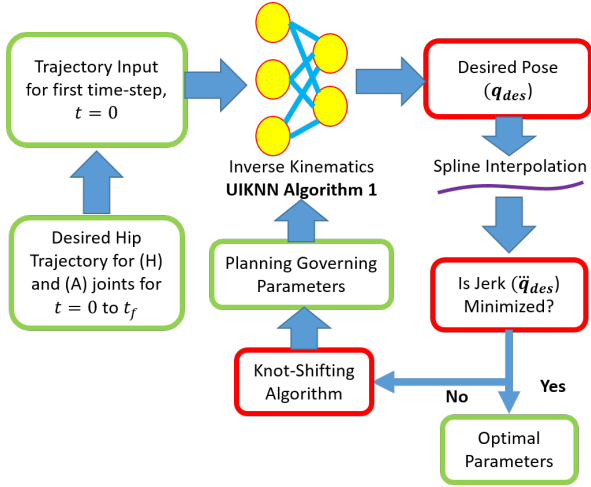


Fig. 5. Knot Shifting IKNN Algorithmic Flow

## VII. CONTACT MODEL FOR GROUND REACTIONS

In comparison to flat foot, toe foot biped model gives more realization to practical human walk mainly during transition from double support phase to single support phase as shown in previous sections for trajectory planning. As we have constraint our model in sagittal plane, so for contact modeling we have considered 6 control points, 3 for each foot; one at toe end, one at sole and one at ankle point.

We have used virtual spring damper model, for modeling the contact forces with parameters  $k_s$ ,  $k_d$  and  $\mu$  which represent the value of spring constant, damping constant and coefficient of friction respectively. These parameters has been taken apriori before the simulation. If  $\mathbf{J}^T$  represents the Jacobian transpose and  $n_c$  denotes the number of control points (6 in our case),  $\mathbf{F}$  denotes the contact forces which have 2 components for  $j^{th}$  control point:

$$F_{n_j} = -k_s \Delta z - k_d \Delta \dot{z} \quad \text{if } \Delta z \leq 0 \quad (33)$$

$$F_{x_j} = \mu F_{n_j} \quad (34)$$

Then extra term is added along with external joint torques given by:

$$\mathbf{B} = \mathbf{J}^T \mathbf{F} \quad (35)$$

where  $\mathbf{J}^T$  is  $9 \times 12$  matrix and  $\mathbf{F}$  is  $12 \times 1$  matrix. where  $\Delta z$  is the difference between ground level and contact point.

## VIII. DYNAMICS MODELING

In previous sections we have planned a staircase trajectory for our Toe Foot Biped robot model and obtained inverse kinematics solution for the same using unsupervised feed forward artificial neural network in real time.

In this section, we are proposing a novel approach for dynamic model where we are combining traditional Lagrange's dynamics with temporal quantization of joint angles based on Inverse kinematics output using artificial neural network. [27] has proposed spatially quantized dynamics for biped robot model but considered Linear Inverted Pendulum Model (LIPM) which is approximation of real dynamics model and

applied spatial quantization to hip trajectory. So to get a improved dynamic model, first, we will calculate Lagrange dynamics for our 9 link toe foot model and then using that dynamics equations, we will model our final Neural Network Temporal Quantized Lagrange Dynamics (NNTQLD) model.

### A. Lagrange Formulation for Dynamics

Euler-Lagrangian or simply Lagrangian formation is based on differentiation of energy terms with respect to system variables and time. It provides equations for getting relationship between position, velocity, acceleration and external force/torque for joint. As we are dealing with only revolute joints, we only need external torque for that joint. For our biped model we have 9 system variables denoted by joint angle vector  $\mathbf{q} = [q_1, q_2, q_3, q_4, q_5, q_6, q_7, q_8, q_9]^T$  where  $q_i : \theta_i, i = 1 \dots 9$  denotes respective joint angle as shown in Fig. 2,  $\dot{\mathbf{q}}$  denotes joint angle velocity vector,  $\ddot{\mathbf{q}}$  represents joint acceleration vector and  $\boldsymbol{\tau} = [\tau_1, \tau_2, \tau_3, \tau_4, \tau_5, \tau_6, \tau_7, \tau_8, \tau_9]^T$  represents external torque vector. Then total kinetic energy  $K$  of our model is function of  $\dot{q}_i$  and total potential energy  $P$  is function of  $q_i$ .

If  $x_{com_i}$  and  $z_{com_i}$  denotes the center of mass position of link  $i$  for  $i = 1 \dots 9$ , then for a particular link, by taking whole mass of link concentrated at center, its kinetic energy is given by:

$$k_i = \frac{1}{2} m_i v_{com_i}^2 + \frac{1}{2} I_i \dot{q}_i^2 \quad (36)$$

where  $m_i$  and  $I_i$  denotes the mass and moment of inertia respectively and  $v_{com_i}$  denotes center of mass velocity for link  $i$  given by:

$$v_{com_i}^2 = \dot{x}_{com_i}^2 + \dot{z}_{com_i}^2 \quad (37)$$

Similarly potential energy for a particular link is given by:

$$p_i = m_i g z_{com_i} \quad (38)$$

where  $g$  denotes gravity constant. Center of mass equations of each link for our model are calculated as per our model.

Then total kinetic and potential energy of our model are given by the following equation:

$$K = \sum_{i=1}^9 k_i \quad \text{and} \quad P = \sum_{i=1}^9 p_i \quad (39)$$

Then, Lagrangian can be defined by following equation:

$$L = K - P \quad (40)$$

Then we can get the following generalized second order ordinary differential equation:

$$\frac{d}{dt} \left( \frac{\partial L}{\partial \dot{q}_i} \right) - \frac{\partial L}{\partial q_i} = \tau_i + B \quad (41)$$

where  $\tau_i$  denotes external torque for link  $i$ .

By solving above equations, we will get final robot equation in following form:

$$\mathbf{M}(\mathbf{q}) \ddot{\mathbf{q}} + \mathbf{C}(\mathbf{q}, \dot{\mathbf{q}}) + \mathbf{G}(\mathbf{q}) = \boldsymbol{\tau} + \mathbf{B} \quad (42)$$

where  $\mathbf{M}(\mathbf{q})$  is  $9 \times 9$  inertia matrix,  $\mathbf{C}(\mathbf{q}, \dot{\mathbf{q}})$  is  $9 \times 1$  coriolis matrix,  $\mathbf{G}(\mathbf{q})$  is  $9 \times 1$  gravity matrix and  $\mathbf{B}$  is the contact model matrix. Robot dynamics has 2 beneficial properties:

- $\mathbf{M}(\mathbf{q})$  is symmetric, bounded and positive definite.
- $\mathbf{M}(\mathbf{q}) \dot{\mathbf{q}} - 2\mathbf{C}(\mathbf{q}, \dot{\mathbf{q}})$  is skew symmetric.

## B. Temporal Quantized Lagrange Dynamics (TQLD)

While calculating inverse kinematics, we are calculating  $\mathbf{q}$  vector value at each time instant by taking time as uniformly quantized parameter given by:

$$t_k = \Delta t \cdot k \quad (k = 0, 1, 2, \dots), \quad (43)$$

where  $\Delta t$  is constant time step. At every time step, state vector  $[\mathbf{q}, \dot{\mathbf{q}}]$  is updated. For each time instant desired joint angles vector (pose vector)  $\mathbf{q}_{des}$  is given by neural network based inverse kinematics and desired joint angles velocity vector (pose velocity vector)  $\dot{\mathbf{q}}_{des}$  is calculated by finite difference method. So for a particular instant  $k$ , equation of motion can be written as:

$$\dot{\mathbf{q}}_{k+1} = \dot{\mathbf{q}}_k + \ddot{\mathbf{q}}_k \Delta t, \quad (44)$$

So, we can now have,

$$\dot{\mathbf{q}}_{k+1} = \dot{\mathbf{q}}_k + \ddot{\mathbf{q}}_k (\Delta T) \quad (45)$$

and

$$\mathbf{q}_{k+1} = \dot{\mathbf{q}}_k (\Delta T) + \frac{1}{2} \ddot{\mathbf{q}}_k (\Delta T)^2 \quad (46)$$

Using equation (42) for particular time instant  $k$  we can have:

$$\ddot{\mathbf{q}}_k = \mathbf{M}^{-1}(\mathbf{q})_k [\boldsymbol{\tau}_k + \mathbf{B}_k - \mathbf{C}(\mathbf{q}, \dot{\mathbf{q}})_k - \mathbf{G}(\mathbf{q})_k] \quad (47)$$

Using equation (47) in (44) and (46), we have updated equations as:

$$\dot{\mathbf{q}}_{k+1} = \dot{\mathbf{q}}_k + \mathbf{M}^{-1}(\mathbf{q})_k [\boldsymbol{\tau}_k + \mathbf{B}_k - \mathbf{C}(\mathbf{q}, \dot{\mathbf{q}})_k - \mathbf{G}(\mathbf{q})_k] \cdot (\Delta T) \quad (48)$$

$$\mathbf{q}_{k+1} = \dot{\mathbf{q}}_k (\Delta T) + \frac{1}{2} \mathbf{M}^{-1}(\mathbf{q})_k [\boldsymbol{\tau}_k + \mathbf{B}_k - \mathbf{C}(\mathbf{q}, \dot{\mathbf{q}})_k - \mathbf{G}(\mathbf{q})_k] \cdot (\Delta T)^2 \quad (49)$$

Equation (48) and (49) combining will give our Temporal Quantized Lagrange Dynamics (TQLD).

---

### Algorithm 3: Temporal Quantized Dynamics

---

**Result:** State Transition

$\boldsymbol{\tau}, \mathbf{q}_C, \dot{\mathbf{q}}_C$  To achieve Next State (N) from Current State (C) ;

$\boldsymbol{\tau} \leftarrow$  Input Torque vector;

$\mathbf{q}_C \leftarrow$  Current Pose Vector;

$\dot{\mathbf{q}}_C \leftarrow$  Current Rate of Change of Pose Vector;

$\mathbf{q}_N \leftarrow$  Next Pose Vector;

$\dot{\mathbf{q}}_N \leftarrow$  Next Rate of Change of Pose Vector;

**while** True **do**

$\ddot{\mathbf{q}}_C \leftarrow$  Dynamics( $\boldsymbol{\tau}, \mathbf{q}_C, \dot{\mathbf{q}}_C$ ) from (45);

$\dot{\mathbf{q}}_N \leftarrow \dot{\mathbf{q}}_C + \ddot{\mathbf{q}}_C \Delta t$  from (46);

$\mathbf{q}_N \leftarrow \mathbf{q}_C \Delta t + \frac{1}{2} \ddot{\mathbf{q}}_C (\Delta t)^2$  from (47);

**end**

**return**  $\mathbf{q}_N, \dot{\mathbf{q}}_N, \ddot{\mathbf{q}}_C$ ;

---

## IX. ZMP STABILITY FORMULATION

The Zero Moment Point (ZMP) based stability is a necessity for performing stable gaits. It is the point where the net moment of all the inertial and gravity forces along axes parallel to ground is equal to zero. The ZMP must lie inside the convex hull formed by the contact points of the biped with the floor and stability margin is defined as the distance of the actual ZMP from the boundaries of the convex hull. The farther the ZMP from all the boundaries, more is the stability margin and it is more feasible to execute the gait. For the SSP, the ZMP must lie within the portion of the stance leg's feet touching the ground whereas, for the DSP, it must be within the supporting polygon formed by all the contact points. The  $x_{ZMP}$  was first formulated for a single mass LIPM model for the kinematic trajectory planning and now, it is assured that the model executes the desired trajectory as much as possible maintaining the actual ZMP considerations, for which  $x_{ZMP}^{actual}$  is calculated as,

$$x_{ZMP}^{actual} = \frac{\sum_{i=1}^n m_i x_i (\ddot{z}_i + g) - \sum_{i=1}^n m_i \ddot{x}_i z_i}{\sum_{i=1}^n m_i (\ddot{z}_i + g) - k \sum_{i=1}^n m_i \ddot{x}_i} \quad (50)$$

where  $\ddot{x}_i$  and  $\ddot{z}_i$  is calculated in Cartesian space from the joint angle accelerations given by (47) in the joint space and  $k$  is the virtual slope considered for modeling the CG motion based on one-mass COG (Center of Gravity) model.

## X. TRAJECTORY TRACKING OPTIMIZATION

In the previous section, the importance of considering the actual ZMP position is already discussed and hence, it is understood that the actual objective is to follow the planned desired trajectory as much as possible along with satisfying the necessary ZMP position limits within the convex hull formed by the contact points with the ground. Thus, torques are to be chosen in a way such that the above objective is achieved.

Hence, the objective function for optimal trajectory tracking is formulated, such that during whole trajectory, the error in the followed trajectory is least deviated from the desired trajectory. This was by achieved by minimizing the tracking error at each time instant  $k$  i.e.

$$\text{Minimize} \sum_{\forall \text{joints}} (\mathbf{q}_k - \mathbf{q}_k^{des})^2 + (\dot{\mathbf{q}}_k - \dot{\mathbf{q}}_k^{des})^2 \quad (51)$$

along with maximizing ZMP Stability Margin based on (47) and subjected to calculating  $\mathbf{q}_k$  and  $\dot{\mathbf{q}}_k$  from equations (48) and (49) for the torques  $\boldsymbol{\tau}_k$ . The optimization problem is solved by the non-linear convex optimization solver *fmincon* in MATLAB.

## XI. RESULT AND DISCUSSIONS

In this section, the simulation results of the considered toe-foot biped model based on the proposed methodology is presented. All the simulations are performed using ©MATLAB and CPU computations on an Intel®i7-7500U CPU@2.70GHz. The simulation consists of a complete up-stairs climbing starting from the first step to gradually climbing the subsequent steps.



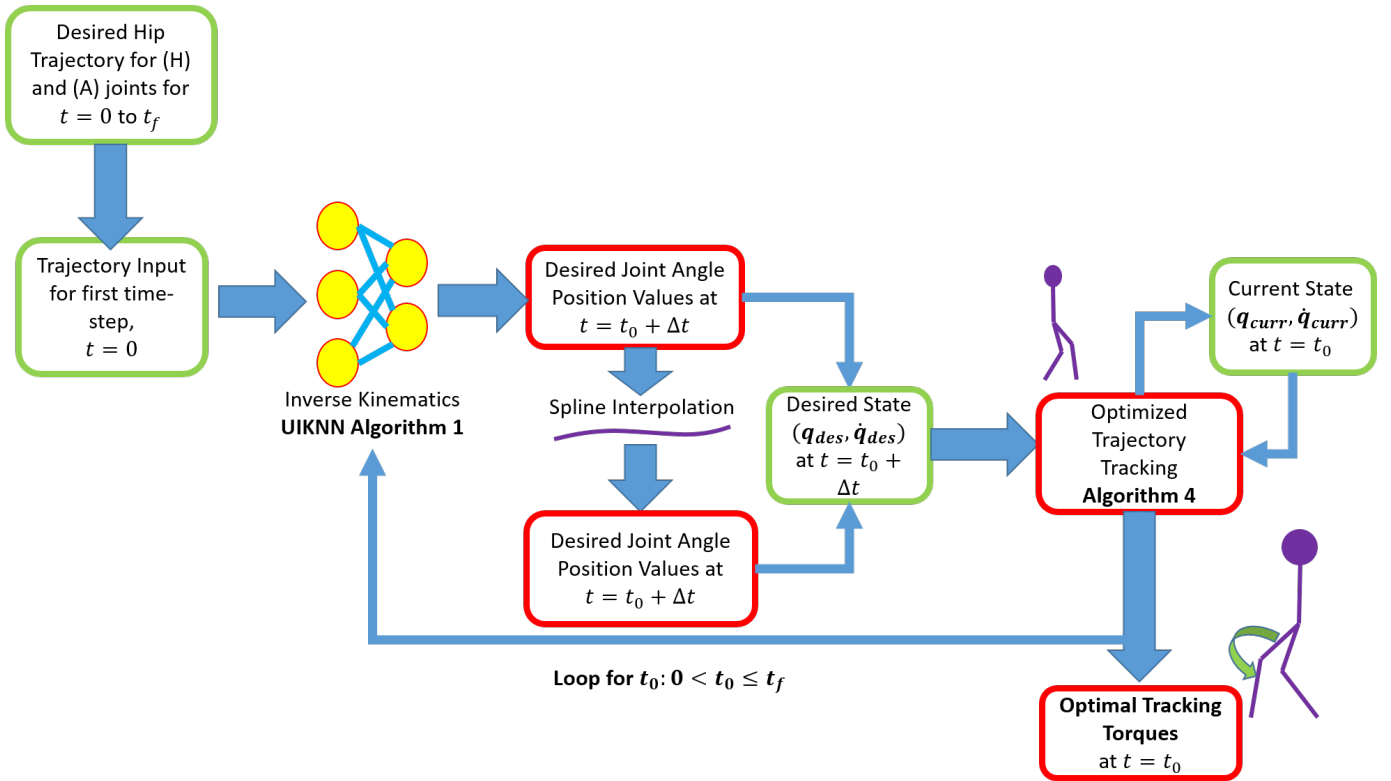


Fig. 6. Complete NNTQLD based Trajectory Tracking Optimization

---

#### Algorithm 4: Satisfying ZMP Constraints

---

**Result:** Satisfy Constraints

$(q_C, \ddot{q}_C)$ ;

$q_C \leftarrow$  Current Pose Vector;

$\ddot{q}_C \leftarrow$  Pose Vector Acceleration;

$x, \ddot{x}, z, \ddot{z} \leftarrow$  Cartesian position and acceleration;

$M \leftarrow$  Weight of all masses;

$ZMP_{fmax} \leftarrow$  Max feasible ZMP position;

$ZMP_{fmin} \leftarrow$  Min feasible ZMP position;

**while True do**

$x, \ddot{x}, z, \ddot{z} \leftarrow func(q_C, \ddot{q}_C)$ ;

$ZMP \leftarrow calculateZMP(M, x, \ddot{x}, z, \ddot{z})$  from (48);

**end**

**return**  $ZMP_{fmin} \leq ZMP \leq ZMP_{fmax}$ ;

---



---

#### Algorithm 5: Trajectory Tracking Optimization

---

**Result:** Determine Optimal Joint Torques

$\tau \leftarrow$  Random Initial Torque;

$q_C \leftarrow$  Current Pose Vector;

$\dot{q}_C \leftarrow$  Current Pose Velocity Vector;

$\ddot{q}_C \leftarrow$  Pose Vector Acceleration;

$q_N^{des} \leftarrow$  Desired Next Pose Vector;

$\dot{q}_N^{des} \leftarrow$  Desired dNext Pose Velocity Vector;

**while True do**

$q_N, \dot{q}_N, \ddot{q}_C \leftarrow StateTransition(\tau, q_C, \dot{q}_C)$ ;

    Minimize  $O_1 = (q_N - q_N^{des})^2 + (\dot{q}_N - \dot{q}_N^{des})^2$  ;

    Such that *SatisfyConstraints*( $q_C, \ddot{q}_C$ ) is True;

    Stop if  $min(O_1)$  is reached for  $\tau_{optimal}$ ;

**end**

**return**  $\tau_{optimal}, q_N^{optimal}, \dot{q}_N^{optimal}$ ;

---

The trajectory planning starts with the Double Support Phase(DSP) of the active leg, as shown in Fig. 3, and gradually gets continued to the Single Support Phase(SSP) based on the knot shifting algorithm in Fig. 5. Based on the knot shifting IKNN optimization the planning governing parameters are obtained as shown in Table III.

Using the optimized parameter values, the trajectory of Hip(H) and Ankle(A) was constructed and Algorithm 2 was used to construct the complete joint angle trajectories. The algorithm would be same in trajectory planning for a single step as well as for the following subsequent steps. The only difference will be the effective length and height of the stairs as upstairs witnesses no change in hip height and a single

step is simulated but for the subsequent steps the double step climbing is accompanied by a rise in hip altitude as well. For the sake of simplicity and due to space constraints, the final algorithm in action is shown for both single and double step climbing whereas the final trajectory values are shown graphically for the double step climbing only.

The only constraint while climbing the first step is that the ZMP-must lie within the span of the stance foot. Thus, it makes climbing the first step relatively easy. Even the movement does not witness any change in the hip altitude. The model considered in the study resembles a lower body framework of a mature male of hip height 80 cm. The effect

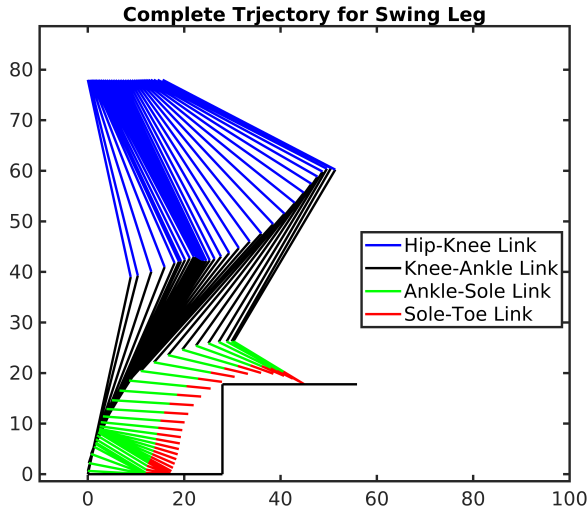


Fig. 7. Bipedal Swing Leg Motion for Upstairs Climbing

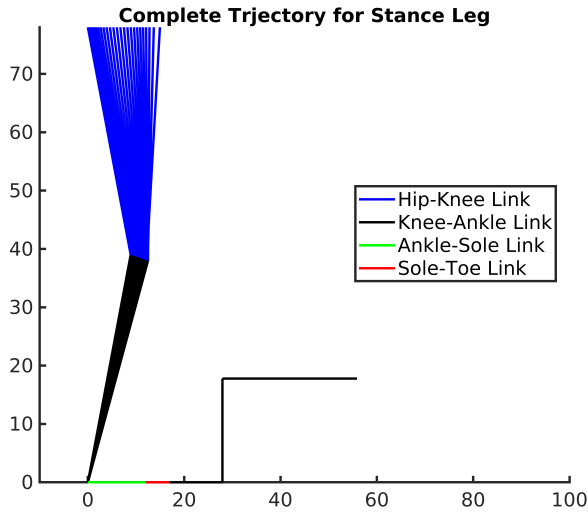


Fig. 8. Bipedal Stance Leg Motion for Upstairs Climbing

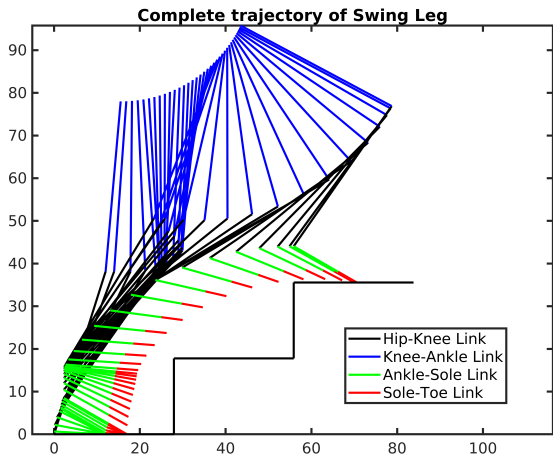


Fig. 9. Bipedal Swing Leg Motion for Subsequent Upstairs Climbing

TABLE III  
OPTIMAL VALUE OF TRAJECTORY GOVERNING PARAMETERS

Parameter	Value	Parameter	Value
$t_1$	0.50 sec	$t_3$	3.50 sec
$t_1^p$	0.80 sec	$\theta_a$	$\pi/6$ rad
$t_2^p$	1.10 sec	$\theta_b$	$\pi/6$ rad
$t_2$	1.40 sec	$\Delta\theta_{c0}$	0.01 rad
$t_{bc}$	2.20 sec	$z_{Ci}$	0.78 meters

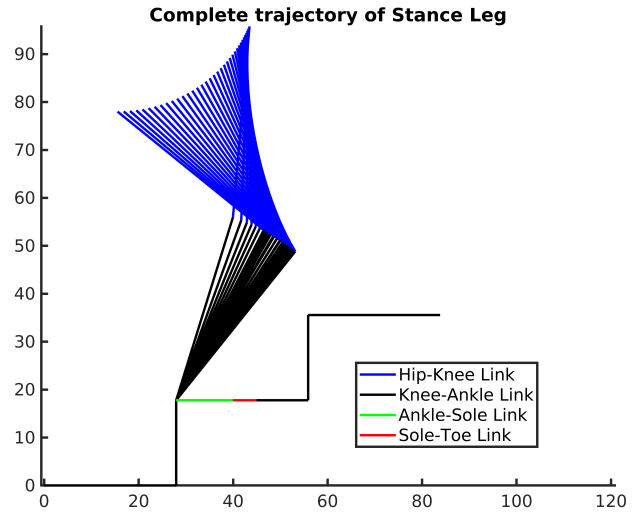


Fig. 10. Bipedal Stance Leg Motion for Subsequent Upstairs Climbing

of considering such a model can be visualized from Fig. 7 where the swing leg combined with a cycloidal realization based trajectory is shown in action.

The corresponding action of the passive leg to support the hip movement accompanying with the active leg swing motion is shown in Fig. 8. The ankle of the stance leg is fixed and moves only after the reverse-DSP for the swing leg finishes. This motion continues to the swing motion for the subsequent step climbing where the passive leg now becomes active and vice-versa.

The stance leg after the completion of the reverse-DSP in the single step phase undergoes a similar planning procedure based on double step climbing targets. The key importance of this phase is to ensure that the ZMP reaches the stance leg foot area on the first step during the DSP such that the model can lift the swing leg maintaining proper stability margin. The importance of proper trajectory governing parameter optimization can be realized where a trade off between the duration of DSP and the position of hip, as soon as the DSP commences, is observed. Furthermore, it should also be noted that during this phase, if the hip moves too far then it may not be possible for a 2 link manipulator with base at hip to follow the desired ankle trajectory. Thus the planning has multiple objectives to satisfy based on the ZMP stability considerations as well as the ankle position must be within the feasible workspace of a 2 link manipulator with its base at the hip as well as satisfying joint angle constraints.

The trajectory for ankle was planned in 3 segments as shown in Fig. 4, namely, the DSP, the Cycloidal segment as well as the

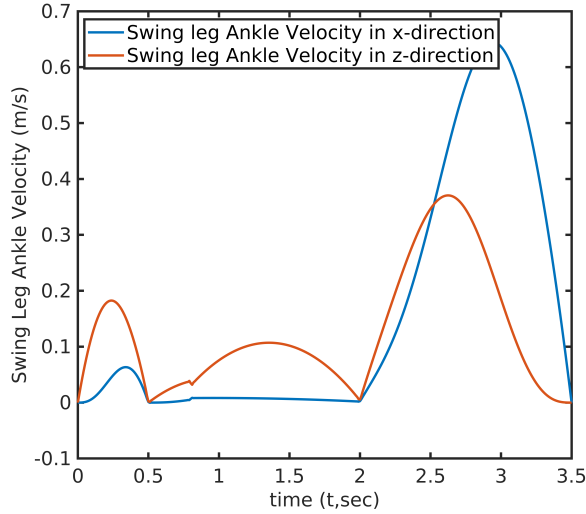


Fig. 11. Swing Leg's Ankle x,z-velocity profile for Subsequent Upstair Climbing

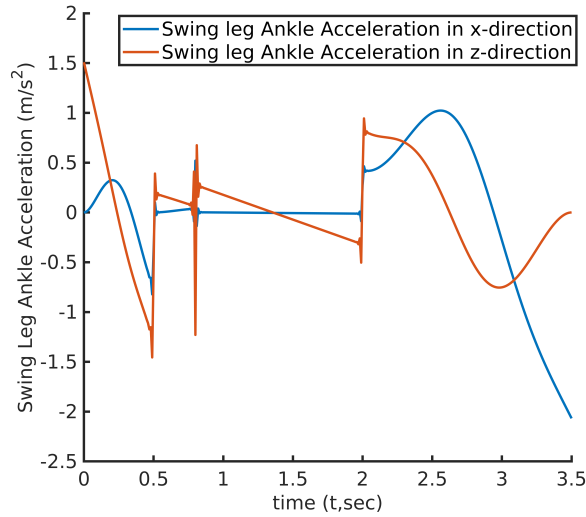


Fig. 12. Swing Leg's Ankle x,z-acceleration profile for Subsequent Upstair Climbing

bezier bridge segment connecting the former two. The control points of the bezier curve are chosen such that it completely meshes with the DSP as well as the cycloid and supports continuity at the transitions.

The overall gait for the subsequent staircase climbing can be visualized in action from Fig. 9 and Fig. 10. The motion of the hip is governed by the fact that x-ZMP must reach the stance leg's foot for transition from DSP to SSP and hence an arc of an inverted circle (center above hip) was used to model the hip motion. Furthermore, the same constraints and objectives as discussed for single step climbing were applicable as well.

The cycloidal realization on staircase supports for smooth velocity and accelerations segments which can be observed after  $t = t_2 = 2.0 \text{ sec}$  can be seen from the x- and z-ankle velocities and accelerations in Fig. 11 and Fig. 12 respectively.

Now, based on the trajectory planning formulations, the Cartesian state vector was transformed into the joint space which is calculated from the hip coordinates as the moving

base. The major joint angles correspond to  $\theta_1, \theta_2, \theta_3, \theta_4$  whereas the other angles vary deterministically like  $\theta_6, \theta_7$  or are constantly 0 like  $\theta_8, \theta_9$  and  $\theta_5 = \pi/2$ , assuming upper body to be always straight upwards. Fig 13 and Fig 14 depicts the corresponding joint angles and joint angle velocities respectively for the major joint angles.

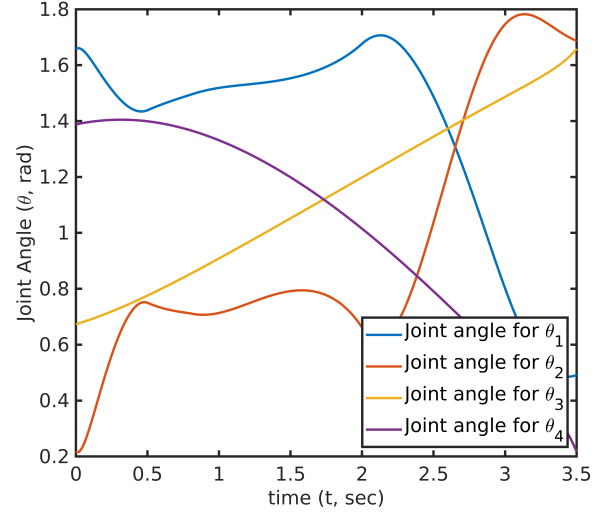


Fig. 13. Joint Space position profile for Subsequent Upstair Climbing

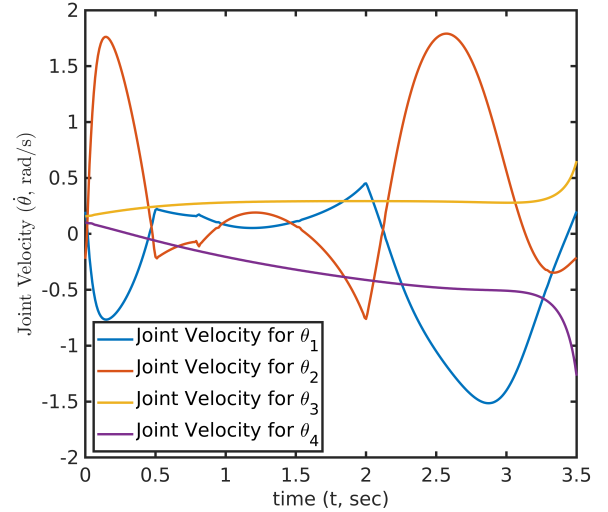


Fig. 14. Joint Space velocity profile for Subsequent Upstair Climbing

The trajectory planning is based on picking, catching and tracking the desired cycloid maintaining various joint constraints along with constraints of stability and workspace limitations. The desired cycloid is planned in order to adapt to a varied range of staircases with different step length and height. This property makes the planning more robust and unique from various previous works. Furthermore, as the desired cycloid is flexible and can be changed at every subsequent step, the planning procedure is very likely to adapt to variable step sizes in a single run as well. The complete simulation can be visualized from the above Fig. 7, Fig. 8, Fig. 9 and Fig. 10, where the first step is climbed and then the motion is planned again for the consecutive step climbing

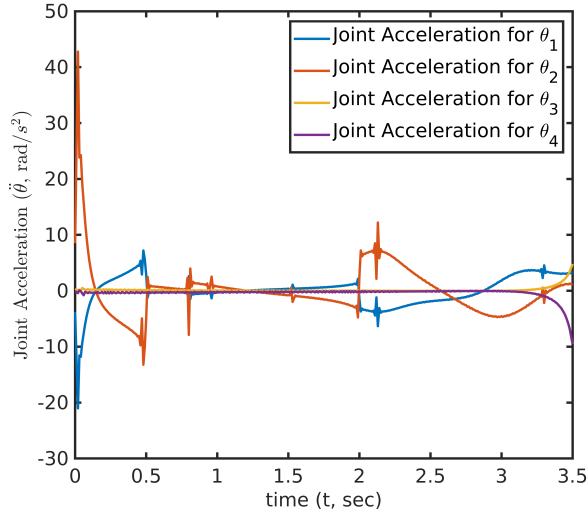


Fig. 15. Joint Space acceleration profile for Subsequent Upstairs Climbing

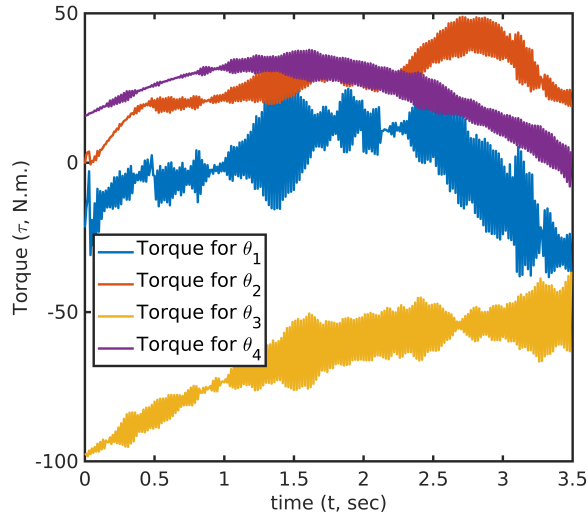


Fig. 16. Joint Torques for Subsequent Upstairs Climbing

and repeated thereafter. Such a method of climbing stairs is more close to natural human walking.

After obtaining the desired joint states i.e. position and velocities, the dynamics equation matrices were obtained and based on the Temporal Quantized Lagrange Dynamics (TQLD) approach further calculations are performed. The complete process can be visualized from the algorithmic flow chart in Fig 6. Based on the trajectory tracking optimization appropriate joint torques were calculated and corresponding joint accelerations are shown in Fig 15. The trajectory tracking torques are given in Fig. 16. Furthermore, with the calculated joint position, velocity and accelerations were transformed to get the Cartesian positions and accelerations which cumulatively gives the x-ZMP. The ZMP trajectory is given in Fig. 17.

Finally, the power consumption for the  $i^{th}$  time step was obtained according to,

$$P_i = |\boldsymbol{\tau}_i \boldsymbol{\omega}_i^T| \quad (52)$$

and was analyzed as shown in Fig. 18. The maximum power

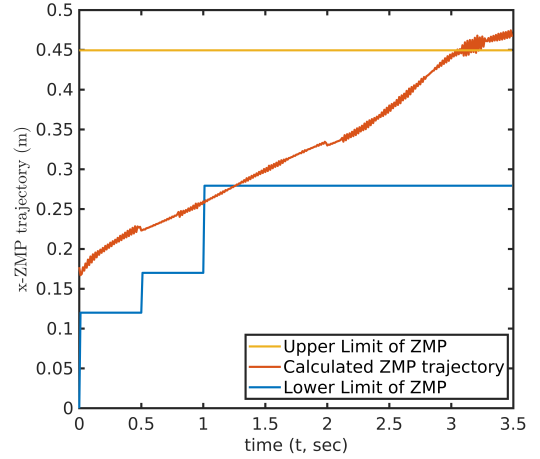


Fig. 17. Observed ZMP trajectory based on NNTLQD for Subsequent Upstairs Climbing

consumption was obtained to be 60.02 W and the overall energy consumption according to,

$$E_{total} = \int_0^{t_f} P_i dt = \int_0^{t_f} |\boldsymbol{\tau}_i \boldsymbol{\omega}_i^T| dt \quad (53)$$

The overall energy consumption for a single subsequent upstairs gait is obtained to be 85.35 Joules.

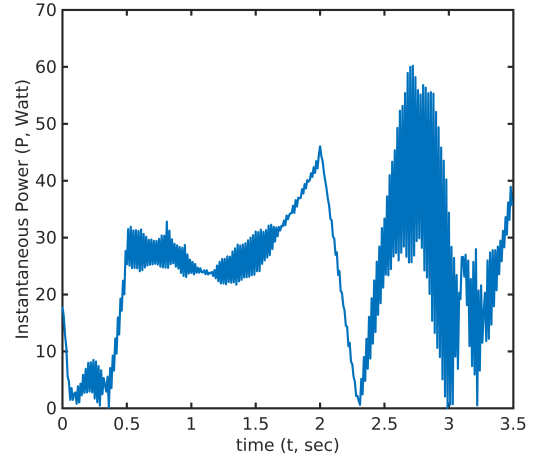


Fig. 18. Observed Instantaneous Power for Subsequent Upstairs Climbing

## XII. CONCLUSIONS

The study presents a novel methodology for a cycloidal realization on upstairs climbing. Cycloidal trajectory has benefits of smooth velocity and acceleration profiles which is desired for serial manipulator movements. Taking the complete planned trajectory as the absolute reference and fitting splines will lead to a lot of enhancements in the smoothing of the curves which is taken as a future challenge by the authors and will be updated in the final manuscript. Coupled with the trajectory planning is the dynamic trajectory tracking which involves the novelty of using Time Quantized Lagrange Dynamics, an approach which tends to simplify the trajectory control torque calculations with small simulation step sizes.

The torques are calculated to give minimum trajectory error and produce joint accelerations capable enough to maintain ZMP-stability. The study concludes with a proper ZMP-Stability analysis, calculation of instantaneous power produced by the actuators as well as overall energy consumption analysis. Future investigations includes completion of various task objectives along with trajectory tracking along with the extension of our model movement into the frontal plane as well.

#### CONFLICT OF INTEREST

The authors declare that they have no conflict of interest.

#### REFERENCES

- [1] Q. Huang, K. Yokoi, S. Kajita, and K. Kaneko, "Planning walking patterns for a biped robot," *IEEE Transactions on Robotics and Automation*, vol. 17, no. 3, pp. 280-289, 2001.
- [2] S. Kajita, F. Kanehiro, K. Kaneko, and K. Fujiwara, "Biped walking pattern generation by using preview control of zero-moment point," *Proc. of IEEE International Conference on Robotics and Automation*, Taipei, Taiwan, Sept 2003.
- [3] C. Zhou and Q. Meng, "Dynamic balance of a biped robot using fuzzy reinforcement learning agents," *Journal of Fuzzy Sets and Systems*, vol. 134, no. 1, pp. 169-187, 2003.
- [4] J. Y. Kim, I. W. park, and J. H. Oh, "Realization of dynamic stair climbing for biped humanoid robot using force/torque sensors," *Journal of Intelligent and Robotic Systems*, vol.56, no. 4, pp. 389-423, 2009.
- [5] C. S. Park, T. ha, J. Kim, and C. H. Choi, "Trajectory generation and control for a biped robot walking upstairs," *International Journal of Control, Automation, and Systems*, vol. 8, no. 2, pp. 339-351, 2010.
- [6] O. Kwona and K. S. Jeon, "Optimal trajectory generation for biped robots walking up-and-down stairs," *Journal of Mechanical Science and Technology (KSME Int. J.)*, vol. 20, no. 5, pp. 612-620, 2-006.
- [7] Shih, C. L., & Chiou, C. J. (1998). The motion control of a statically stable biped robot on an uneven floor. *IEEE Transactions on Systems, Man, and Cybernetics, Part B: Cybernetics*, 28(2), 244-249.
- [8] Jeon, K. S., Kwon, O., & Park, J. H. (2004). Optimal trajectory generation for a biped robot walking a staircase based on genetic algorithms. *2004 IEEE/RSJ International Conference on Intelligent Robots and Systems (IROS)*, 3(1), 2837-2842. <https://doi.org/10.1109/iros.2004.1389839>.
- [9] Morisawa, M., Kajita, S., Kaneko, K., Harada, K., Kanehiro, F., Fujiwara, K., & Hirukawa, H. (2005). Pattern generation of biped walking constrained on parametric surface. *Proceedings - IEEE International Conference on Robotics and Automation*, 2005(April), 2405-2410. <https://doi.org/10.1109/ROBOT.2005.1570473>.
- [10] Sato, T., Sakaino, S., Ohashi, E., & Ohnishi, K. (2011). Walking trajectory planning on stairs using virtual slope for biped robots. *IEEE Transactions on Industrial Electronics*, 58(4), 1385-1396. <https://doi.org/10.1109/TIE.2010.2050753>.
- [11] Gutmann, J. S., Fukuchi, M., & Fujita, M. (2004). Stair climbing for humanoid robots using stereo vision. *2004 IEEE/RSJ International Conference on Intelligent Robots and Systems (IROS)*. <https://doi.org/10.1109/iros.2004.1389593>
- [12] De Lope, J., Gonzalez-Careaga, R., Zarraonandia, T., & Maravall, D. (2004). Inverse kinematics for humanoid robots using artificial neural networks. *Lecture Notes in Computer Science (Including Subseries Lecture Notes in Artificial Intelligence and Lecture Notes in Bioinformatics)*, 2809(January), 448-459. [https://doi.org/10.1007/978-3-540-45210-2\\_41](https://doi.org/10.1007/978-3-540-45210-2_41).
- [13] Husty, M. L., Pfulner, M., & Schrocker, H. P. (2007). A new and efficient algorithm for the inverse kinematics of a general serial 6R manipulator. *Mechanism and Machine Theory*, 42(1), 66-81. <https://doi.org/10.1016/j.mechmachtheory.2006.02.001>.
- [14] Almusawi, A. R. J., Dulger, L. C., & Kapucu, S. (2016). A New Artificial Neural Network Approach in Solving Inverse Kinematics of Robotic Arm (Denso VP6242). *Computational Intelligence and Neuroscience*, 2016. <https://doi.org/10.1155/2016/5720163>.
- [15] Duka, A.-V. (2014). Neural Network-based Inverse Kinematics Solution for Trajectory Tracking of a Robotic Arm. *Procedia Technology*, 12, 20-27. <https://doi.org/10.1016/j.protcy.2013.12.451>.
- [16] Chen, S., Mulgrew, B., & Grant, P. M. (1993). A Clustering Technique for Digital Communications Channel Equalization Using Radial Basis Function Networks. *IEEE Transactions on Neural Networks*, 4(4), 570-590. <https://doi.org/10.1109/72.238312>.
- [17] Takanishi, A., Ishida, M., Yamazaki, Y., & Kato, I. (1985). REALIZATION OF DYNAMIC WALKING BY THE BIPED WALKING ROBOT WL-10RD.
- [18] Panwar, R., & Sukavanam, N. (2018). Trajectory tracking using an artificial neural network for stable human-like gait with upper body motion. *Neural Computing and Applications*. <https://doi.org/10.1007/s00521-018-3842-1>.
- [19] Kajita, S., Kanehiro, F., Kaneko, K., Fujiwara, K., Yokoi, K., & Hirukawa, H. (2003). Biped walking pattern generation by a simple three-dimensional inverted pendulum model. *Advanced Robotics*. <https://doi.org/10.1163/156855303321165097>
- [20] Kuo, A. D., Donelan, J. M., & Ruina, A. (2005). Energetic consequences of walking like an inverted pendulum: Step-to-step transitions. *Exercise and Sport Sciences Reviews*. <https://doi.org/10.1097/00003677-200504000-00006>
- [21] Kajita, S., Kanehiro, F., Kaneko, K., Yokoi, K., & Hirukawa, H. (2001). The 3D linear inverted pendulum mode: A simple modeling for a biped walking pattern generation. *IEEE International Conference on Intelligent Robots and Systems*. <https://doi.org/10.1109/iros.2001.973365>
- [22] Rostami, M., & Bessonnet, G. (2001). Sagittal gait of a biped robot during the single support phase. Part 2: Optimal motion. *Robotica*, 19(3), 241-253. <https://doi.org/10.1017/S0263574700003039>.
- [23] Vukobratovic, M. (1972). Contribution To the Study of Anthropomorphic Systems. *Kybernetika*, 8(5), 404-418.
- [24] Goswami, A. (1999). Postural Stability of Biped Robots and the Foot-Rotation Indicator (FRI) Point. *The International Journal of Robotics Research*, 18(6), 523-533. <https://doi.org/10.1177/02783649922066376>.
- [25] Hirukawa, H., Hattori, S., Harada, K., Kajita, S., Kaneko, K., Kanehiro, F., Fujiwara, K., & Morisawa, M. (2006). A universal stability criterion of the foot contact of legged robots - Adios ZMP. *Proceedings - IEEE International Conference on Robotics and Automation*, 2006(May), 1976-1983. <https://doi.org/10.1109/ROBOT.2006.1641995>.
- [26] C.H. Irvine, S.H. Snook, J.H. Sparshatt, Stairway risers and treads: acceptable and preferred dimensions, *Applied Ergonomics*, Volume 21, Issue 3, 1990, Pages 215-225, ISSN 0003-6870, [https://doi.org/10.1016/0003-6870\(90\)90005-1](https://doi.org/10.1016/0003-6870(90)90005-1)
- [27] Kajita, S., Benallegue, M., Cisneros, R., Sakaguchi, T., Nakaoka, S., Morisawa, M., Kaneko, K., & Kanehiro, F. (2017). Biped walking pattern generation based on spatially quantized dynamics. *IEEE-RAS International Conference on Humanoid Robots*. <https://doi.org/10.1109/HUMANOIDS.2017.8246933>